Multistability of reentrant rhythms in an ionic model of a two-dimensional annulus of cardiac tissue

Philippe Comtois*
Research Centre, Montreal Heart Institute and Department of Pharmacology, McGill University, Montreal, Quebec H3G 1Y6, Canada

Alain Vinet
Department of Physiology and Institute of Biomedical Engineering, Université de Montréal and Research Centre, Hôpital du Sacré-Coeur, Montreal, Quebec H4J 1C5, Canada

(Received 10 January 2004; revised manuscript received 8 December 2004; published 29 November 2005)

The dynamics of reentry in a model of a two-dimensional annulus of homogeneous cardiac tissue, with a Beeler-Reuter type formulation of the membrane ionic currents, is examined. The bifurcation structure of the sustained propagated solutions is described as a function of R_{in} and R_{out}, the inner and outer radii of the annulus. The transition from periodic to quasiperiodic reentry occurs at a critical R_{in}, which first diminishes and then saturates as R_{out} is increased. The reduction of the critical R_{in} is a consequence of the increase of the wave-front curvature. There is a range of R_{in} below the critical radius in which two distinct quasiperiodic solutions coexist. Each of these solutions disappears at its own specific value of R_{in}, and their annihilation is preceded by a new type of bifurcation leading to a regime of propagation with transient successive detachments of the wave front from the inner border of the annulus.

DOI: 10.1103/PhysRevE.72.051927 PACS number(s): 87.19.Hh, 05.45.−a

I. INTRODUCTION

Cardiac reentry, referring to the self-sustained propagation of a wave of excitation in the tissue, is an important mechanism generating cardiac arrhythmias. Since the seminal paper of Mines [1] on an experimental model of reentry, transient or sustained reentry has been shown to occur around an anatomical obstacle or around a region of partially or totally inexcitable tissue [2–5]. In continuous two- and three-dimensional media, reentry, in the form of a spiral wave, has been obtained both numerically and experimentally without the requirement of anatomical or inexcitable obstacles [6–11]. Such spiral waves are thought to play a role in both initiating [12,13] and sustaining fibrillation [14,15].

Self-sustained propagation in a continuous one-dimensional (1D) ring is the simplest model of reentry around an obstacle [16–18]. For large radii, stable period-1 reentry exists, corresponding to a fixed wave form traveling at constant speed around the annulus. Decreasing the length of the pathway may change propagation to quasiperiodic reentry if the restitution curve, which describes the duration of the action potential duration (APD) as a function of the recovery time, is an increasing function with a slope >1 at low recovery intervals [19,20]. However, even when this condition is fulfilled, periodic propagation may remain stable if memory and/or electrotonic effects are important [21–23].

A previous paper [24] has suggested that bifurcation from period-1 to quasiperiodic reentry could also occur in the annulus [25], but the characteristics of the bifurcation were not investigated in detail. The main difference between the 1D ring and the 2D annulus is the existence of the curved activation and repolarization front, which follows from their extension from the inner to outer radius of the annulus. It is well known that increased curvature of the activation front reduces the velocity of propagation [26–28], and it has been shown that the curvature can also prolong the duration of the action potential [29]. However, not much is known about the influence of these mechanisms on the stability of anatomical reentry.

This paper has two main results. First, we present a detailed description of the bifurcation of sustained reentry as a function of the inner and outer radii of the annulus. Two different types of bifurcation occur in different ranges of radii: first, a transition from period-1 to quasiperiodic solutions and then, at a still shorter inner radius, a transition to quasiperiodic solutions with repetitive transient unpinning of the activation front from the inner border of the annulus. The analysis of the bifurcation is done for two versions of the membrane ionic model, which differ in the duration of action potential and its rhythm dependence.

The second result is a comparison of the dynamics of the full 2D annulus model with a simplified formulation. The simplified model deals with period-1 reentry, for which the spatial profile of the activation front is described by a set of ordinary differential equations. Then, the stability of the solution is established by solving a reaction-diffusion system describing the propagation at $r=R_{in}$. The pseudo-2D reaction-diffusion system is also used to examine the quasiperiodic regimes of reentry. Comparing the behavior of the 2D and simplified models helps to clarify the contribution of the curvature of the activation front, of the action potential restitution curve, and of the velocity dispersion curve to the stability of the sustained reentry. This is also a preliminary step toward a simplified model that could reproduce all the

*Corresponding author. Electronic address: p-comtois@crhsc.rtss.qc.ca

regimes of reentry in the annulus, as has been done with an integral-delay model in the 1D ring [17,19,20,31,38].

II. MODELS

Two different models of the annulus are used in this paper. The first and more general model is a 2D reaction-diffusion equation, while the second model is a reduction of the first model.

A. Reaction-diffusion model

The model is based on the monodomain reaction-diffusion equation, which, in polar coordinates, is written as

$$\frac{\partial^2 V}{\partial r^2} + \frac{1}{r}\frac{\partial V}{\partial r} + \frac{1}{r^2}\frac{\partial^2 V}{\partial \phi^2} = \rho S\left(C_M \frac{\partial V}{\partial t} + I_{ion}\right), \tag{1}$$

where V is the transmembrane potential (mV), C_M is the membrane capacitance ($1\ \mu\mathrm{F/cm}^2$), S is the surface-to-volume ratio of the intracellular medium ($0.4\ \mu\mathrm{m}^{-1}$), ρ is the intracellular resistivity (200 Ω cm), and I_{ion} is the ionic current ($\mu\mathrm{A/cm}^2$). Neumann boundary conditions are imposed on both the inner boundary ($r=R_{in}$) and the outer boundary ($r=R_{out}$) such that

$$\left.\frac{\partial V}{\partial r}\right|_{R_{in}} = \left.\frac{\partial V}{\partial r}\right|_{R_{out}} = 0.$$

Numerical solutions are obtained using the spectral-finite element method described in the Appendix.

B. Simplified kinematical model

The simplified model is a two-step procedure: First, the kinematical model described in Comtois and Vinet [29] is used to obtain the form of the activation front for period-1 reentry in the annulus. The kinematical model is based on the assumptions that, in period-1 reentry, (1) the activation and repolarization fronts extending from $r=R_{in}$ to $r=R_{out}$ are identical and (2) their velocity vector is tangent to the annulus at $r=R_{in}$ and $r=R_{out}$. The curve describing the form of the activation and repolarization fronts across the annulus is obtained by solving the system of ordinary differential equations

$$\frac{dD}{ds} = \frac{f}{h},$$

$$\frac{dK}{ds} = \frac{f}{\theta_K}\left(1 - \frac{\theta_D}{h}\right),$$

$$\frac{d\nu}{ds} = K\theta, \tag{2}$$

where s is the curvilinear coordinate along the front ($s=0$ at $r=R_{in}$), $D(s)$ is the diastolic interval, $K(s)$ is the local curvature, and θ and $v(s)$ are, respectively, the speed normal and tangent to the front. The model is based on a generalized APD restitution relation $A(K,D)=A_\infty(K)F(D)$, giving the APD as a function of the local diastolic interval $D(s)$ and of the local curvature $K(s)$, and a general velocity dispersion relation $\theta(K,D)=\theta_\infty(K)F_2(D-D_{min}(K))$. The notation $Y_x = \partial Y/\partial x$ is used to represent the partial derivative of the dispersion and restitution relations (i.e., $\theta_D, \theta_K, A_D, A_K$). The function $f=\omega-K\nu$, where $\omega=2\pi R_{in}/\theta(K(s=0),D(s=0))$, is the constant angular velocity of the period-1 reentry, and $h=\theta_D-\theta_K(A_D+1)/A_K$. The functions $A(K,D)$ and $\theta(K,D)$ and the method to solve the system are given in [29]. The derivatives of the two functions $A_\infty(K)$ and $F(D)$ defining the duration of the action potential are both positive, such that augmenting the curvature and/or the diastolic interval prolongs the duration of the action potential $A(K,D)$. On the other hand, $\theta_\infty(K)=\theta_0-\mu K$ is a decreasing function, while $F_2(u)$ and $D_{min}(K)$ are both increasing functions. Increasing the curvature therefore reduces the speed through $\theta_\infty(K)$ and through the increase of the minimum diastolic interval $D_{min}(K)$ in $F_2(u)$ that sets the minimum value of D below which the propagation stops. The kinematical model has a unique solution for each pair of values $[R_{in},R_{out}]$, in which the curvature is always maximum and positive at $r=R_{in}$.

In the second step $K_{in}=K(s=0)$, the curvature of the period-1 solution at R_{in}, obtained from the kinematical model, is introduced as a parameter in the pseudo-two-dimensional system:

$$\frac{1}{R_{in}^2}\frac{\partial^2 V(\phi,t)}{\partial \phi^2} + \frac{K_{in}}{R_{in}}\frac{\partial V(\phi,t)}{\partial \phi} = \rho S\left(C_M \frac{\partial V(\phi,t)}{\partial t} + I_{ion}(\phi,t)\right). \tag{3}$$

This equation is deduced from Eq. (1) by assuming that (1) all the equipotential curves $V(r,\phi)=c$ are identical so that the spatial variation of curvature along them is the same; (2) the propagation is normal to r, which is true at $r=R_{in}$ and $r=R_{out}$; and (3) the curvature is constant in time, which is true for period-1 solutions. It is the first assumption that makes Eq. (3) an approximation of Eq. (1). This pseudo-2D model is equivalent to the 1D cable equation, supplemented by an advection term that introduces the effect of curvature at R_{in}. The equation is solved as a 1D cable equation of length $L=2\pi R_{in}$ with periodic boundary conditions [18] using a finite-element method with linear basis functions on a uniform grid with an internode distance of 50 μm and a constant 5-μs time step [29]. It can give a stable period-1 reentry, a sustained quasiperiodic solution, or a transient reentry leading to annihilation.

In summary, the kinematical model predicts what should be the curvature of the activation front in a period-1 reentry. The pseudo-2D system is then used to diagnose the stability of this period-1 solution. Together, they provide a simplified alternative to be compared with the complete reaction-diffusion model defined by Eq. (1).

C. Ionic model

The membrane ionic current I_{ion} is represented by a Beeler-Reuter-type model [30] described in [18,20,31]. The model is identical to the original Beeler-Reuter formulation, except for the sodium current $[I_{Na}=g_{Na}m^3hj(V-E_{na})]$. The

variables m and h follow the Drouhard-Roberge formulation [36], while $j_\infty(V)=h_\infty(V)$ and $\tau_j(V)=10\tau_h(V)$. The Beeler-Reuter-Drouhard-Roberge (BRDR) model was chosen because its properties have been extensively documented both in the 1D ring [18,20,32] and in the space-clamped configuration [33–35] and because the generalized dispersion and restitution relations needed for the kinematical model have been previously obtained [29]. In the BRDR model, the APD is determined by an interplay between the outward potassium current and the slow inward calcium current $[I_{si}=g_{si}df(V-E_{si})]$. I_{si} is controlled by one "activation" variable (d) and one "inactivation" variable (f), each of which is characterized by a time constant $(\tau_d(V),\tau_f(V))$ and a steady-state function $(d_\infty(V),f_\infty(V))$. In this paper, comparison is made between the BRDR model, in which the time constants are set as in [30], and the modified BRDR (MBRDR) model where $\tau_d(V)$ and $\tau_f(V)$ are halved. Halving the time constants abbreviates the action potential and has been shown to change the bifurcation structure both in the space-clamped configuration and in the 1D ring [36,38].

Simulations of the two reaction-diffusion systems defined by Eqs. (1) and (3) give the variation of V in time and space [see Fig. 1(a)]. Each active response is associated with the formation of an action potential [Fig. 1(b)]. For each node, the activation time is defined as the instant when $|dV/dt|$ reaches its maximum during the upstroke, and the repolarization time, marking the end of the action potential and the beginning of the diastolic interval, is taken as the moment of the downcrossing of −50 mV during repolarization (corresponding approximately to 70% of repolarization or APD70). The time interval between two successive activations (T) is divided in two parts: the action potential duration (A), from the activation time to the following repolarization time, and the diastolic interval (D), from the repolarization time to the next activation time. Since the APD restitution curve and velocity dispersion relation are most often given as functions of D and since D is also the independent variable in low-dimensional models developed to represent the dynamics of paced cells and reentry in the 1D ring, we display the spatial profile of D to describe the propagation.

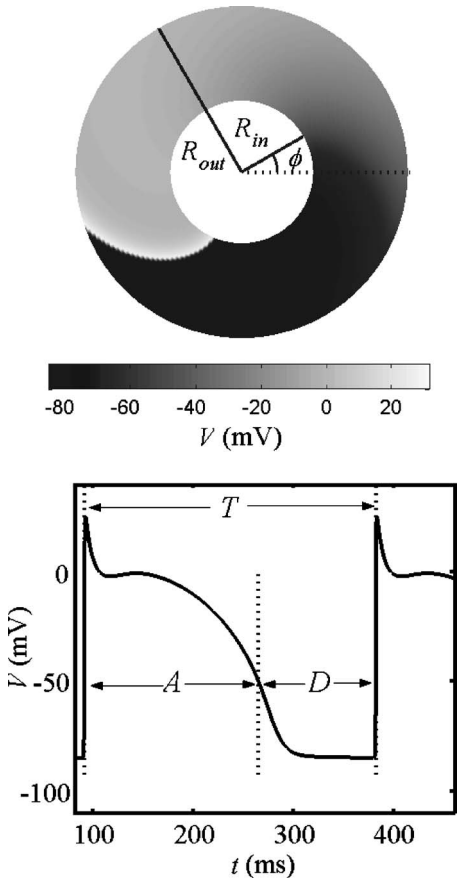

FIG. 1. Reaction diffusion model: (A) Wave front of period-1 reentry in an annulus with $R_{in}=3.0$ cm and $R_{out}=7.0$ cm. The gray scale depicts the transmembrane potential V. (B) Action potential at $r=R_{in}$. The period T is the time between successive activations, A is the action potential duration (APD), and the diastolic interval $D=T-A$.

III. RESULTS

A. Increasing the width of the annulus: Formation of a curved wave front

In a 1D ring, period-1 reentry remains stable as long as the radius is larger than a critical value [18,31]. On the annulus, the stability of the period-1 solution depends on both R_{in} and R_{out}. Figure 2 shows the effect of $\Delta R=R_{out}-R_{in}$ on the period-1 solution in an annulus with $R_{in}=3.05$ cm. The widening of ΔR prolongs the period of the rotation [T, Fig. 2(a)], until T saturates at $\Delta R\approx 0.35$ cm. The curves in Fig. 2(b) present the angular position of the activation front as a function of $r'=r-R_{in}$ for different ΔR. The slope of these curves at $\phi=0$ mirrors the curvature of the front at $r=R_{in}$. It shows that the curvature increases as ΔR is widened, but saturates, as did the value of T, at $\Delta R\approx 0.35$ cm.

The kinematical model defined by Eq. (2) was found to fit closely the spatial profile of the activation front and the spatial distribution of D, as well as the value T of the period-1 solutions of the BRDR reaction-diffusion model for all R_{in} and R_{out}. The kinematical model provides $K(s)$ and $D(s)$, and permits an examination of the interplay of the mechanisms responsible for the slowing of the propagation. The widening of ΔR increases $K_{in}=K(0)$, so that the speed of propagation is reduced both through the eikonal velocity relation $\theta_\infty(K)$ [27] and through an increase of the absolute refractory period $D_{min}(K)$ in $F_2(D-D_{min}(K))$. This second contribution reflects the fact that for a higher curvature a more excitable medium is needed for propagation to be sustained. However, K_{in} always remains less than 3.0 cm^{-1} for the period-1 solutions at all the values of R_{in} and ΔR considered in this article, so that the change of $D_{min}(K)<1$ ms can be neglected. Hence, for a constant value of R_{in}, widening ΔR increases K_{in}, which results in a reduction of $\theta_\infty(K)$ and a prolongation of T. Since $T=D+A(D)$, the effect of K_{in} on the speed and the period is partially counterbalanced by the increase of D.

B. Transition from periodic to quasiperiodic reentry

In the BRDR 1D ring model, propagation changes from period-1 to quasiperiodic reentry when the radius is reduced

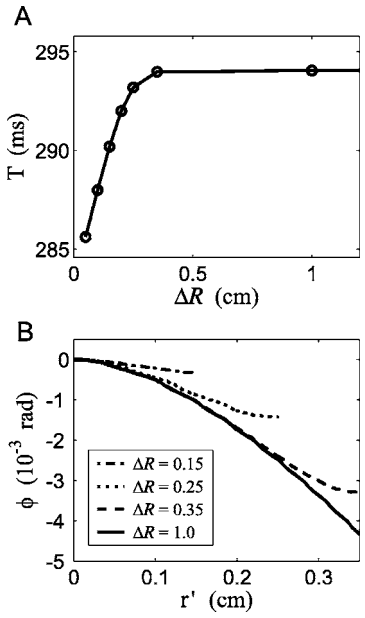

FIG. 2. BRDR reaction-diffusion model: (A) Period of rotation (T) of the period-1 solution as a function of the width ΔR of an annulus with $R_{in}=3.05$ cm ($T=284.5$ ms for $\Delta R=0$, the 1D ring). The increase of T saturates at $\Delta R \approx 0.4$ cm. (B) Angular position of the wave front, for different values of ΔR. The position of the wave front is defined as the value of ϕ where $|\partial V/\partial \phi|$) reaches its maximum for each $r'=r-R_{in}$, with the position at R_{in} taken as reference ($\phi=0$). The initial deflection of the wave front (at $r' \approx 0$) increases with ΔR, but also saturates at $\Delta R \approx 0.35$ cm.

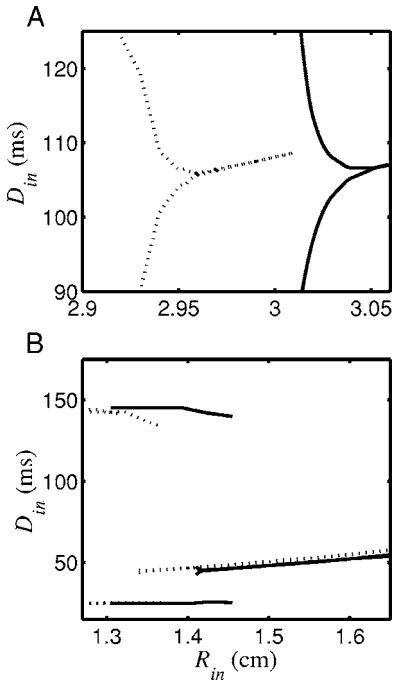

FIG. 3. BRDR and MBRDR reaction-diffusion models: The bifurcation as a function of R_{in} for two different widths of the annulus: $\Delta R=0.05$ cm (solid curves) and $\Delta R=1.0$ cm (dotted curves). The minimum and maximum D measured at R_{in} for each stable solution are plotted. The bifurcation of the BRDR model is supercritical (A), while it is subcritical for the MBRDR model, with bistability between period-1 and quasiperiodic solutions (B).

below a critical value $R_{in,crit}$ [17–20,38]. This section investigates how the width of the annulus acts upon this bifurcation.

To study the bifurcation, ΔR was kept constant and R_{in} was decreased with a minimum step of 0.001 cm. To diagnose the stability, the values of D were collected for all nodes at $r=R_{in}$ for three complete rotations. If the differences between the successive values at each node were less than 0.5 ms, the system was considered to be in a stable period-1 regime. If this criterion was not satisfied, but if the differences between the successive maxima and between the successive minima of D were both less than 0.5 ms, the system was considered to be in a quasiperiodic regime. The calculation was continued until one of these sets of criteria was fulfilled. The final stable solution was then mapped on the next annulus (smaller R_{in}, same ΔR) as initial condition. The reverse procedure (increasing R_{in}) was done to investigate bistability near the bifurcation.

The process was repeated for different values of ΔR to track the bifurcation in the $[R_{in}, \Delta R]$ parameter plane. $\Delta R=0.05$ cm was the first and smallest value investigated. For this case, the initial R_{in} was chosen large enough to give a stable period-1 solution on a 1D ring and the initial condition was built by pasting together the 1D ring solutions for each value r between R_{in} and R_{out}, with a shift in the angular position to reproduce the curvature of the activation front. The shift was taken from the solution of the kinematical model. Afterward, for each larger values of ΔR, the results from the annulus with the closest shorter ΔR already studied were used to build a new initial condition. A value of R_{in} giving a stable period-1 solution was selected, and the corresponding stable solution was mapped onto the new annulus with the same R_{in} and the larger new ΔR value. R_{in} was again changed gradually to locate the bifurcation.

Figure 3(a) (BRDR model) shows the results for two values of ΔR. Increasing the width of the annulus from $\Delta R=0.05$ cm (solid curve) to $\Delta R=1.0$ cm (dotted curve) yields the same bifurcation from period-1 to quasiperiodic solution, but at different values of $R_{in,crit}$ (from 3.05 to 2.95 cm, compared to 3.1 cm for the 1D ring). The D spatial profile of these quasiperiodic solutions displays oscillations whose amplitude increases as R_{in} is diminished below $R_{in,crit}$. The bifurcation is supercritical since there is a gradual increase of the amplitude of the oscillation and no bistability between period-1 and quasiperiodic solutions [39]. Figure 4 (dashed curve) provides a global picture of the locus of the bifurcation in the $[R_{in}, \Delta R]$ parameter plane. $R_{in,crit}$ reaches an asymptotic minimum value for $\Delta R \approx 0.5$ cm, for a total decrease of approximately 0.15 cm (from 3.1 cm in the 1D ring down to 2.95 cm in the 2D annulus) [20,31]. Hence increasing the width of the annulus stabilizes the period-1 reentry since the transition to quasiperiodic propagation is shifted to a lower $R_{in,crit}$. The inset in Fig. 4 shows that the period of rotation at $R_{in,crit}$ remains almost constant for all ΔR values, a key observation to explain the mechanism responsible for the bifurcation.

The pseudo-2D equation, fed with the K_{in} values obtained from the kinematical model, gives a relatively accurate pre-

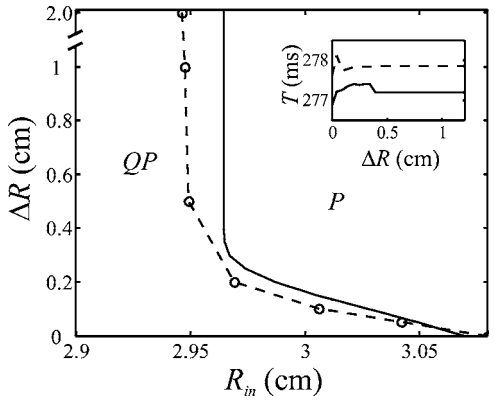

FIG. 4. The boundary between period-1 (P) and quasiperiodic (QP) reentry in the $(R_{in},\Delta R)$ parameter plane for the BRDR model. The boundary defines a curve $[\Delta R(R_{in,crit})]$, which is similar for the reaction-diffusion model (dashed curve) and the combination of the kinematical [Eq. (2)] and pseudo-2D [Eq. (3)] modes (solid curve). Inset: The period of rotation at the bifurcation for both models is approximately constant as a function of ΔR.

diction of $R_{in,crit}$ as a function of ΔR and the same invariance of T at the bifurcation (Fig. 4 and inset, solid curves). Hence we can use the kinematical model to analyze the characteristics of the solutions at the bifurcation. Since K_{in} was always <3 cm^{-1} for all bifurcations from period-1 to quasiperiodic solutions, the term $A_\infty(K)$ in the function $A(K,D)=A_\infty(K)F(D)$ giving the APD varied by less than 1 ms, and A can be approximated as a function of D alone [i.e., $A(D)=A_\infty(0)F(D)$]. In period-1 reentry, $T=A+D$. Since the bifurcation occurs at the same critical value of period T_{crit} for all ΔR, it also occurs at a constant value D_{crit}, which fulfills the relation $T_{crit}=A(D_{crit})+D_{crit}$. In fact, D_{crit} is close to the value where the slope of $A_\infty(0)F(D)$ is equal to 1.0 [98 ms for $A_\infty(0)F(D)$, while $D_{crit}=106$ ms for the two cases shown in Fig. 3(a)]. This indicates that the slope of the restitution curve with respect to D is still the main determinant of the stability of the period-1 reentry in the BRDR annulus model, as it was in the case of the 1D ring [19,20]. D_{crit} and T_{crit} being determined by the slope of the restitution curve, $R_{in,crit}(\Delta R)$ is given by the relation

$$\frac{2\pi R_{in,crit}(\Delta R)}{T_{crit}} = \theta_\infty(K(R_{in,crit}(\Delta R),\Delta R)) \times F_2(D_{crit} - D_{min}(K(R_{in,crit}(\Delta R),\Delta R))).$$

The 1D ring corresponds to $\Delta R=0$ and $K(R,0)=0$. Neglecting the variation of D_{min} and using $\theta_\infty(K)=\theta_0-\mu K$ yields

$$\frac{R_{in,crit}(\Delta R)}{R_{in,crit}(0)} = 1 - \frac{\mu}{\theta_0}K(R_{in,crit}(\Delta R),\Delta R), \quad (4)$$

where μ, θ_0, and $K(R_{in},\Delta R)$ depend on the resistivity of the medium and on the characteristics of I_{Na} activation. In the BRDR 1D ring model, $R_{in,crit}(0)=3.1$ cm and $\theta_0=70.29$ cm. In our previous work with the pseudo-2D formulation [29], we obtained estimates for $\mu=1.05$ cm^2/sec and

$$K(R_{in},\infty) \approx 5.1e^{-0.62R_{in}} + 1.8e^{-0.02R_{in}}. \quad (5)$$

Solving together Eqs. (4) and (5) gives the unique solution $R_{in,crit}(\infty)=2.98$ cm, which is the smallest R_{in} at which the bifurcation can occur since the effect of ΔR on the curvature at R_{in} is maximal when $\Delta R\to\infty$. In spite of the approximation made in the fitting given in Eq. (5), it is close to the value obtained by numerical simulation of the kinematical and pseudo-2D model (2.97 cm). As seen in Fig. 4, the limit of the reaction-diffusion model is a little lower, at $\sim$2.95 cm. Since the simulations of the pseudo-2D model use the $K_{in}(R_{in})$ value predicted by kinematical model, which is based on restitution and dispersion functions obtained by fitting, this could explain some part of the discrepancy. However, the basic assumption of the pseudo-2D model, which is that all equipotentials have the same curvature, certainly contributes to the difference with the complete 2D model.

In summary, the stability of the period-1 solution of the BRDR model is determined by D_{crit}, the value at which the slope of the APD $[\approx A_\infty(0)F(D)]$ restitution curve reaches 1. In this model, $D_{crit}\approx 98$ ms and falls in a range where the D-dependent term of the speed of propagation is still constant and maximal [illustrated in Fig. 5(e)], so that the variation of curvature is the only factor that can decrease the speed of propagation (through the term $\theta_0-\mu K$) and shorten $R_{in,crit}$. The high value of D_{crit} also forces the bifurcation to occur in a range of R_{in} where K_{in} remains relatively small (less than 3 cm^{-1} in the kinematical model), even for a large annulus.

The dynamics of the MBRDR model has been described both in the paced space-clamped configuration and 1D ring [35,38]. Because the MBRDR model has a shorter APD, the loss of stability of the period-1 solution is taking place at a shorter period of repetitive activity, associated with a shorter ring radius. The bifurcation is subcritical, with an interval of bistability between period-1 and period-2 solutions in the space-clamped configuration, and period-1 and quasiperiodic (QP) reentry in the 1D ring. This change from supercritical to subcritical bifurcation was explained by the increase in the steepness of the APD restitution curve induced by the acceleration of the dynamics of d and f gates. The same type of behavior is seen in the annulus. $R_{in,crit}$ is much smaller for the MBRDR model [Fig. 3(b)], and the bifurcation becomes subcritical, with an interval of R_{in} in which period-1 and quasiperiodic reentries coexist. As for the BRDR model, $R_{in,crit}$ is reduced by the increase of ΔR, until it reaches a saturated value. The fact that the transition from supercritical to subcritical bifurcation also occurs in the annulus indicates that the steepness of the restitution relation still controls the bifurcation.

C. Existence of multiple-QP solutions in the BRDR model

Two different QP modes of reentry have been observed in the 1D ring [18,31,36]. Labeled as mode-0 and mode-1 (associated, respectively, with the first and second eigenvalues of the integral-delay equation used to analyze the system), they differ both in their spatial period and in the way they are created. The fact that only a finite number of modes exist and

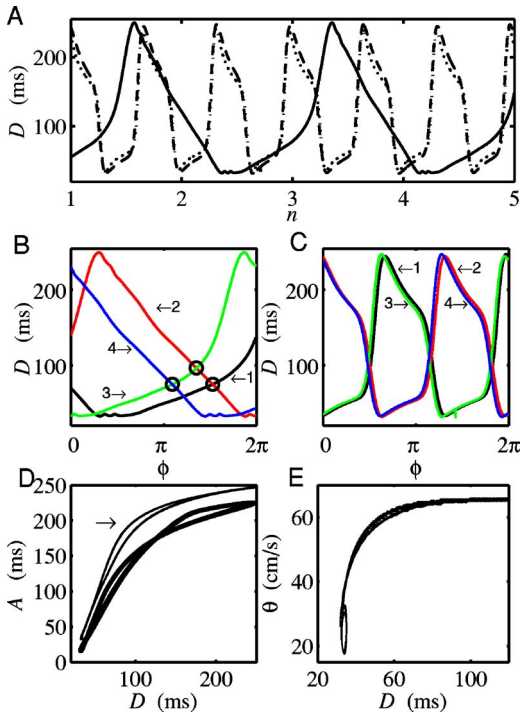

FIG. 5. (Color online) Quasiperiodic modes of reentry in the BRDR reaction-diffusion model: (A) $\Delta R=2.0$ cm: mode-0 ($R_{in}=2.09$ cm, solid line) and mode-1 ($R_{in}=2.42$, dashed line) solutions at R_{in}. The curves represent the values of D at each site along $r=R_{in}$ for multiple turns (n) abutted end to end. The dotted curve represents D at $r=R_{out}$ for mode-1 and is almost identical to D at $r=R_{in}$, showing that the variation is concordant along r. (B) Variation of D along ϕ for 4 successive turns [$n=1$, 2, 3, and 4, respectively black, red, green, and blue (color in online version)] of the mode-0 solution. Each pair of successive turns is associated with a single node (crossing between high and low values highlighted by circles). (C) Same as in panel (B), but for mode-1, which gives three nodes. (D) The restitution curves $A(D)$ for mode-0 (thin lines pointed to by the arrow with $D_{min}=31$ ms, $dA/dD|_{max}=3.5$, and $D_{crit}=95$ and 106 ms for derivative of the lower branch and upper branch, respectively) and mode-1 (thick line with $D_{min}=31$ ms, $dA/dD|_{max}=3.2$, and $D_{crit}=98$ and 130 ms) from the quasiperiodic solutions displayed in panel (A). For clarity, the mode-0 curve is upshifted by 20 ms. Each curve has two branches, corresponding, respectively, to the increasing and decreasing phase of D [31]. (E) The dispersion curves $\theta(D)$ of the two solutions are superimposed.

that they are appearing at different values of the radius was argued to be a consequence of the effect of resistive coupling on the APD [20]. As in the 1D ring, the bifurcation in the MBR annulus is supercritical and the quasiperiodic solution that appears at the bifurcation always corresponds to the mode-0 solution. As shown in Fig. 5(a) (thick curve), the profile of D has a spatial period that is close to two-turns. The bifurcation being supercritical, our method of investigation that starts from a period-1 reentry and does a continuous tracking of the solution as a function of ΔR could only provide information of the evolution of the mode-0 solution. To obtain the mode-1 solution, an alternative initial solution had to be constructed. Mode-1 solutions were available from our previous work on the 1D ring [18,31,38]. One of these solutions was mapped onto each radius of the annulus, with a shift in the angular position (taken from the period-1 solution predicted from the kinematical model for the same annulus). For a given ΔR, this procedure was first tried for an annulus with $R_{in}=R_{in,crit}$ and repeated with shorter values of R_{in} until a stable mode-1 solution was found. The characteristics of the mode-1 solution were then investigated by the procedure of continuous decrease and increase of R_{in}. We found that the mode-1 solution [Fig. 5(c), $R_{in}=2.42$] appears at $R_{in}<R_{in,crit}$ (e.g., for $\Delta R=2$ cm, $R_{in}\approx 2.82$ cm$<R_{in,crit}=2.95$ cm) with a high-amplitude oscillation of D and a spatial wavelength ~ 3 times shorter than the mode-0 solution. The two modes are thus created by distinct scenarios of bifurcation that occur at different values of R_{in}.

In the examples presented in Fig. 5, the wavelength of the mode-0 solution is ~ 1.75 turns, so that the profile of D has a single maximum and/or minimum for each turn [Fig. 5(b)]. As a consequence, each successive pair of turns defines a single node (transition from high to low D values or vice versa) whose value and location changed continuously owing to the quasiperiodic nature of the propagation. The mode-1 solution, with a wavelength of ~ 0.67 turns, has three nodes [Fig. 5(c)]. Each mode of quasiperiodic propagation also produces its own A-vs-D restitution curve [Fig. 5(d): mode-0, thin curve, and mode-1, thick curve]. Each curve has two branches, which are associated, respectively, with the phase of the propagation in which A and D increase or decrease. This reflects the modulating effect of the electrotonic coupling on the APD [20,31]. On the other hand, the two modes have almost the same $\theta(D)$ dispersion curve [Fig. 5(e)].

The MBRDR model produces quasiperiodic solutions that are different from the BRDR model, but that are similar to those observed in the 1D ring [38]. The bifurcation is subcritical, with bistability between period-1 reentry and quasiperiodic reentry, which appears with high amplitude D oscillations [Figs. 3(b) and 6(a)]. The APD as a function of D is shown in Fig. 6(b). The APD and the minimum D value are shorter than for the BRDR model, and the high-slope portion is more abrupt and is restricted to a smaller interval of D near D_{min}. Since the quasiperiodic solution appears with high-amplitude D oscillations, it covers as soon as it is created a range of D where the slope of both the restitution and dispersion curves [see Fig. 6(c)] are important. We have suggested that the complexity of the spatiotemporal pattern of D was resulting from the interaction of the high-slope regions of the restitution and dispersion curves [37].

D. Dynamics of wave-front unpinning

In the 1D BRDR ring model, the quasiperiodic solutions disappear below a minimum radius when the activation front blocks in its refractory tail (for the BRDR model, at $R_{in}=2.04$ cm) [18,19,36]. If $\Delta R<\Delta R_{min}$ (~ 0.25 cm for mode-0 and ~ 0.65 cm for mode-1), the sustained reentry disappears in the BRDR annulus as in the 1D ring [18,31,38]. However, for $\Delta R\geqslant\Delta R_{min}$, a new form of sustained reentry appears at low R_{in}. The wave front unpins from the obstacle, with the formation of a phase singularity (PS, defined as the end point

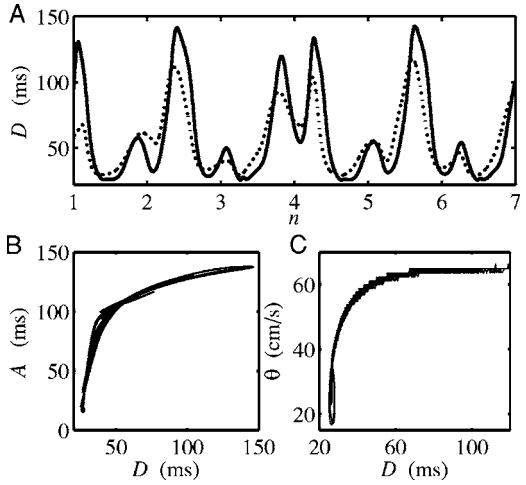

FIG. 6. (A) The MBRDR has only one quasiperiodic mode of reentry. It shows complex and modulated oscillation of D with an amplitude that is slightly less at $R_{out}=3.27$ (dotted line) than at $R_{in}=1.27$ cm (solid line). (B) $A(D)$ ($D_{min}=25$ ms, D_{crit} falling between 42 and 52 ms for the slope of the different branches, and $dA/dD|_{max}=10$) obtained with the quasiperiodic mode in panel (A) for which the maximum APD is shorter, but the slope steeper than in the BRDR model. (C) The dispersion curve $\theta(D)$ for the solution displayed in panel (A) is identical to the dispersion curve obtained for the BRDR model [Fig. 5(e)].

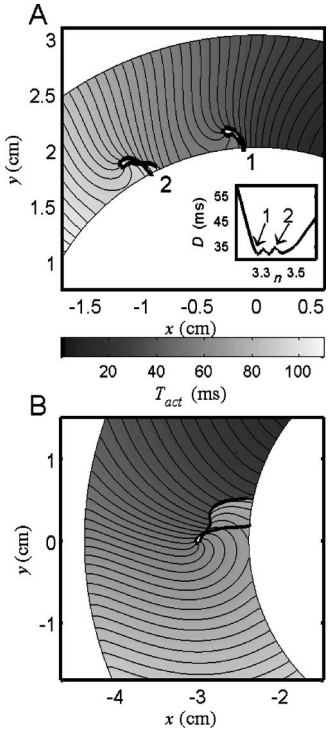

FIG. 7. BRDR model. (A) Unpinning for the mode-0 quasiperiodic reentry ($R_{in}=2.022$ cm and $\Delta R=1.0$ cm) occurs twice (labeled 1 and 2) at positions corresponding to closely spaced minima of D (shown in the inset for $r=2.522$ cm). (B) Unpinning for the mode-1 reentry ($R_{in}=2.415$ cm and $\Delta R=2$ cm) first occurs once at each turn, at the position where D is below a minimum threshold value, but the sequence becomes increasingly complex with time.

of a wave front that is not attached to a boundary) that makes an excursion in the interior of medium and then reattaches to the inner border. This behavior is found for both the BRDR and MBRDR ionic models. The unpinning introduces a delay in the period of rotation that allows the propagation to remain sustained at shorter values of R_{in}.

Examples of wave unpinning for the mode-0 and mode-1 quasiperiodic solutions of the BRDR model are shown in Fig. 7. The wave propagates around the annulus (the thin black curves are the isochrones of activation taken at 5-ms intervals) to reach a locus where the excitability at the inner border is too low to sustain the propagation. The wave front stops near $r=R_{in}$, but the medium at some distance away from the inner border is still excitable enough to maintain the propagation. The activation front travels around the region of functional block, reattaches to the inner border, and continues its propagation until the next unpinning. The block is clearly due to a lack of excitability near the inner border and not to the curvature of the front reaching a critical value, since the excitation front is almost rectilinear at the site of block and reaches quite a high curvature when it travels around the inexcitable region.

For the mode-0 reentry, unpinning first appears at $R_{in} \approx 2.04$ cm, which is close to the minimum radius for mode-0 reentry in the 1D ring model [31]. Below a minimum R_{in} ($R_{min} \approx 2.02$ cm), wave unpinning and quasiperiodic reentry can no longer produce a sustained propagation. The successive detachments rather create a sequence of retrograde and antegrade fronts that finally lead to the annihilation of reentry. For mode-1, unpinning first occurs at $R_{in} \approx 2.48$ cm (compared to the termination of mode-1 reentry at ~ 2.52 cm when $\Delta R=0$), a value at which mode-0 still propagates without detachment. Sustained propagation stops through a transient fibrillatorylike activity when R_{in} is decreased to ~ 2.45 cm.

The two modes (mode-0 and mode-1 of the BRDR model) of propagation also differ with respect to the dynamics of the unpinnings.

For mode-0 [Fig. 7(a), $R_{in}=2.022$ cm and $\Delta R=1.0$ cm], the wave unpins twice at two positions spaced by only 5.2% of one rotation. Accordingly, the spatial profile of D at $r=R_{in}$ has two closely spaced minima at the positions where the detachments occur [inset in Fig. 7(a)]. The wave front then reattaches to the obstacle and propagates for a distance corresponding to the wavelength of the D oscillation (~ 1.67 turn) before the next sequence of unpinning. For mode-1 [Fig. 7(b)], the unpinning occurs once at every 1.34 turn [~ 2 times the wavelength of mode-1 as illustrated in Fig. 5(a)] with a much more complex dynamics. Instead of repetitive detachments with similar trajectories of the PS as in mode-0, we have observed a very long transient (>200 turns) during which the maximum distance traveled by the PS increased slowly from one unpinning to the next, a process of amplification leading to an irregular but sustained pattern.

The quasiperiodic reentry of the MBRDR model differs from both the mode-0 and mode-1 QP reentry of the BRDR model, as already seen in Figs. 5 and 6. The two types of unpinning, occurring, respectively, for the mode-0 and mode-1 reentries in the BRDR model, are now observed to-

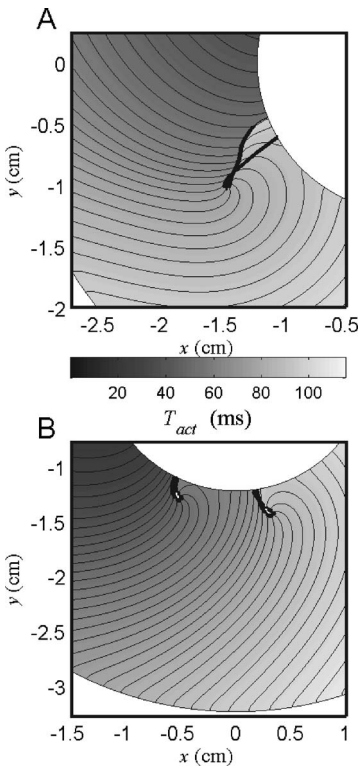

FIG. 8. Two types of wave-front unpinning from the obstacle coexist for the MBRDR model with $R_{in}=1.226$ cm and $\Delta R=2.0$ cm (isochrones of activation time at each 2.5 ms are shown as thin lines). (A) The wave tip of the broken front travels along a single long trajectory (thick black line) or (B) a series of two smaller trajectories.

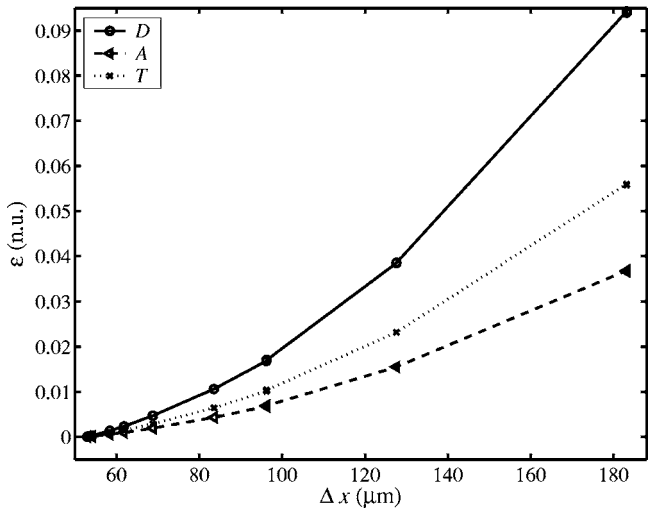

FIG. 9. Effect of spatial discretization $[\Delta x=2\pi R_{in}/(N-1)$ with $R_{in}=3.5$ cm] on the normalized error ($\varepsilon=[d-\min(d)]/\min(d)$ normalized units (n.u.), where $\min(d)$ is the results obtained with $N=2^{12}$) for $d\in\{D,A,T\}$ of a period-1 reentry with $\Delta R=2$ cm. The number of layers along r is $N_r=250$.

gether during the same reentry. The single unpinning depicted in Fig. 8 for $R_{in}=1.226$ cm is the first to appear (starting at $R_{in}=1.28$ cm and $\Delta R_{min}>0.6$ cm), with a dynamics similar to that of the mode-1 solution of the BRDR model. The front blocks at $r=R_{in}$, and the PS can reenter in the area of block at $r\sim R_{in}+0.75$ cm. The second type of unpinning, with two consecutive detachments as shown in Fig. 9, appears at $R_{in}=1.228$ cm when $\Delta R=2$ cm and is similar to the unpinning of the mode-0 quasiperiodic reentry of the BRDR model in which the wave front detaches twice during the same rotation. The minimum width of the annulus ($\Delta R_{min}\approx 0.2$ cm) is again slightly less than for the single unpinning as is the case for the BRDR model. Elucidating the details of the bifurcation would require further study. However, the results suggest that the acceleration of the d and f gates leads to a merging of the mode-0 and mode-1 solutions (a single mode exists in the MBRDR model) into a single regime that combines some characteristics of both regimes (the two types of unpinning are present).

IV. DISCUSSION

A. Loss of stability of periodic reentry

The bifurcation from period-1 to quasiperiodic reentry in the annulus retains all the major features observed in the 1D ring for both the BRDR and MBRDR models. For the BRDR model, the bifurcation remains supercritical, with the appearance and then gradual gain of the amplitude of a mode-0 solution. A second mode-1 solution is created at a lower radius, where it appears with high amplitude. For the MBRDR model, the bifurcation is subcritical, with a single complex nonperiodic solution. The preservation on the annulus of all these features, which were shown in the 1D ring to be dependent on the APD restitution curve, as well as the fact that the bifurcation always occurs at the same critical period T_{crit} and D_{crit} irrespective of the value of R_{out}, indicate that the slope of the restitution curve is still the major determinant of the stability in these models. The only difference introduced by the width of the annulus is the decrease in $R_{in,crit}$, associated with the slowing of the propagation induced by the curvature of the front. Although, in principle, the interaction of curvature with the APD and the minimum D for propagation can also have an influence, these effects remain negligible in the BRDR and MBRDR models.

Because we are considering a continuous system, the conclusions about the nature of the bifurcation do not depend on the properties of the medium. The medium is fully characterized by a space constant $\lambda=\sqrt{1/g_m\rho S}$ and the time constant $\tau=g_mC_m$, in which g_m is the resting membrane resistivity. Equation (1) can be made nondimensional by defining the radial and temporal coordinates $r_0=r/\lambda$ and $t_0=t/\tau$. The characteristics of the bifurcation in any specific medium can then be obtained by rescaling those obtained in the nondimensional systems. The values of $R_{in,crit}$ and ΔR are proportional to $\rho^{-1/2}$, but the values of T_{crit} and D_{crit} are invariant with respect to ρ. They rather depend on the membrane properties of the medium.

The ability of the pseudo-2D formulation to reproduce the location of the bifurcation of the BRDR model also helps to understand the dynamics. The difference between the pseudo-2D and the complete 2D model regarding stability of the period-1 solution is that the latter includes implicitly the

perturbations affecting the curvature, in addition to those related to the diastolic interval. Although it has been established that curvature can destabilize a spiral wave from a circular core to a meandering trajectory [40], the equivalence of the two models shows that instability that could be associated with fluctuations of the curvature *per se* does not contribute to the destabilization of the period-1 reentry in the BRDR annulus.

However, we do not have any means to circumscribe precisely the class of membrane ionic model for which this conclusion would remain true. Evidently, for any model, we can repeat the procedure of obtaining the general restitution and dispersion relations (i.e., function of D and K) and then perform the comparison between the complete reaction-diffusion model and the simplified model. Even if this procedure can provide useful information, it does not allow any general prediction. What is needed is a simplified formulation, in the spirit of the integral-delay model for the 1D ring [19,20,31], that will allow a formal analysis of the factors acting on the bifurcation. Nevertheless, our results indicate that an integral-delay model describing the propagation at $r=R_{in}$ based on generalized restitution and dispersion relations and complemented by functional description of $K_{in}(R_{in},\Delta R)$ would be sufficient to describe the characteristics and the stability of the period-1 solution bifurcation for at least a subclass of cardiac ionic models.

However, a simplified approach to describe quasiperiodic propagation with high-amplitude D oscillations, but still no unpinning, would need to incorporate the spatiotemporal variation of K_{in} during propagation. The notion of critical curvature may also need to be updated. This concept was first introduced to define the maximum curvature corresponding to the critical ratio of source/sink for suprathreshold activation [27]. But it should also include the fact that the minimal excitability for propagation depends on both the morphology of the wave and the spatial distribution of prematurity [29]. The question about the importance that this effect has on reentry dynamics remains open.

The annulus geometry has been used previously to study the dynamics of the Luo-Rudy I (LR-I) ionic model [25]. Qu *et al.* argued that an increase in the width of the annulus shifted the transition from period-1 to quasiperiodic reentry to a higher inner radius. They explained the loss of stability by the formation of "transverse modes" [41] or discordant alternans far from R_{in}. These conclusions are the opposite of our results, which show that a larger ΔR allows stable period-1 reentry at lower R_{in} and that stability can be predicted from a simplified model describing the dynamics at $r=R_{in}$. Although quasiperiodic solutions may be viewed as discordant alternans in the angular direction [see Figs. 5(a) and 5(b) and Fig. 6(a)], we have always observed the oscillations of D to occur together and in phase from $r=R_{in}$ to $r=R_{out}$, although the amplitude of the oscillations was slightly reduced at $r=R_{out}$.

To understand this discrepancy, we first investigated the conditions to obtain discordant alternans in the BRDR ionic model. Concordant and discordant alternans can be generated in a paced cable when the maximum slope of the restitution curve is greater than 1 [42]. Generally, discordant alternans appear only if the length of the cable is beyond a minimum value [43], and an even greater dimension is required in a 2D medium [15]. A BRDR cable [with the same ρ and S as in Eq. (1)] was paced at one end at a period of stimulation just below the value of T_{crit} for transition to quasiperiodic propagation in the annulus. We found discordant alternans when the length of cable was greater than 5 cm. This value is far beyond the values of ΔR and R_{out} studied in this article (see Fig. 4), which makes it unlikely that discordant alternans may form along the radial direction for the small and intermediate ΔR studied herein.

We then repeated our procedure (change R_{in} with ΔR fixed) to identify the locus of the bifurcation with the version of the Luo-Rudy I model used by Xie *et al.* [25]. As for the BRDR model, we found the bifurcation to occur at lower R_{in} for larger values of ΔR ($\sim$2.3 cm for $\Delta R=1.0$ compared to $\sim$2.4 cm for $\Delta R=0.05$ cm). Furthermore, we also found the bifurcation of the Luo-Rudy I model to be supercritical, which eliminates the possibility that the conflict between our results and those Xie *et al.* was spawned by a difference in the methods used to localize the bifurcation in a case where there would be bistability between period-1 and quasiperiodic solutions. The only remaining avenue that we still envision to reconcile the two set of results is that a new type of bifurcation, involving discordant alternans along the radial direction, may take place when the medium becomes extended enough, this being consistent with the fact that most of the results shown by Xie *et al.* were obtained on an annulus with a ΔR value of 9.2 cm. Further investigation is needed to unravel this hypothesis.

B. Dynamics of wave-front unpinning

In the 1D ring model, quasiperiodic reentry stops when the activation front reaches a portion of the medium that is still refractory. In the 2D annulus, annihilation is preceded by new regimes of propagation specific to each mode of quasiperiodic propagation. Detachment of the wave front from the obstacle arises because the refractoriness is greater at the inner border than elsewhere in the medium. The wave can propagate beyond this zone of block because the tissue remains excitable at some distance from the obstacle, thus creating a transient functional reentry. This type of propagation is similar to the meandering of a spiral wave in a continuous medium without an obstacle [9,10,15]. Both the initiation and evolution of wave-front unpinning are governed by the localized dynamics near the inner radius. This localization near R_{in} is somewhat similar to the meandering mechanism near the circular core of a spiral wave described by Otani [44] or to the concept of the sensitive zone of a spiral wave [45]. Herein, the dynamics of the wave-front unpinning depends on spatiotemporal variations of excitability specific to each quasiperiodic mode of propagation.

When the system is set in a regime of sustained unpinning, diminishing R_{in} leads to an annihilation of reentry through a complex dynamics that can be designated as a transient fibrillation. For the BRDR model, both the duration and dynamical features of this transient fibrillation depend on the quasiperiodic mode from which it has been induced. It is known that the BRDR and MBRDR models cannot pro-

duce stable reentry in a 2D sheet [37]. Sustained vortices can be obtained only if the acceleration factor of the d and f gates is greater than the value of 2 that we have used in this paper. For higher values of the acceleration factor, it might be possible to get a transition from quasiperiodic reentry to sustained fibrillation by diminishing R_{in}.

However, our results with an acceleration factor of 2 suggest that a unique quasiperiodic solution will then exist below $R_{in,crit}$. A more interesting situation would be a model with multiple modes of quasiperiodic reentry also allowing sustained fibrillation. Since the different modes would be likely to disappear at different R_{in}, this will raise the possibility of bistability between quasiperiodic reentry and fibrillation in the annulus. It will also allow examination of whether the multiple modes of quasiperiodic reentry can be used to induce fibrillations with different dynamical signatures (e.g., frequency content), raising the possibility that fibrillation characteristics could also be set by the "initial conditions" of the substrate, in addition to differences in tissue electrophysiology [46].

V. CONCLUSIONS

This work illustrates that the BRDR and MBRDR formulations belong to the class of models for which the stability of the period-1 solution is controlled in the first place by the restitution curve of the APD, which reaches high slope at values of D where the D-dependent part of the propagation speed is still maximum and constant. The high D also compels the bifurcation to occur at a large value of R_{in}, where the curvature is still low. The most interesting situation will obviously be a model in which the bifurcation will occur with high curvature as well as high slope of the restitution and dispersion relations. However, it is still to be seen whether such a regime can be reached with a realistic cardiac model. Our results also stress how misleading a study of bifurcation can become without some *a priori* knowledge of the possible dynamical regimes that may exist in the system. In our case, the mode-1 solution of the BRDR model would have been missed, if we had not been guided by our prior investigation of the 1D ring. Beside, a larger rate of ΔR reduction could have also lead to detecting a direct transition from period-1 to mode-1 quasiperiodic reentry. It would also have been difficult to identify what aspects of the dynamics were truly a consequence of the 2D extension of the annulus had not the space-clamped, 1D ring and the pseudo-2D settings been previously investigated. The next challenging step is to produce a simplified 2D formulation that would allow some general analytical discussion of all the regimes of propagation on the 2D annulus.

ACKNOWLEDGMENTS

We thank Dr. M Guevara (McGill University, Montreal, Canada) for editorial comments. This work was supported by grants from the Natural Sciences and Engineering Research Council of Canada (A.V.) and the "Fonds Québécois de la Recherche sur la Nature et les Technologies" (P.C.), as well as by the technical and computer resources of the "Réseau Québécois de Calcul de Haute Performance."

APPENDIX: NUMERICAL METHOD

Simulation of Eq. (1) is done by first expressing the partial derivative in time as a forward finite difference:

$$\frac{\partial V}{dt} = \frac{V^t - V^{t-\Delta t}}{\Delta t}, \tag{A1}$$

where V and $V^{t-\Delta t}$ are, respectively, the potential at time t and $t-\Delta t$. Introducing Eq. (A1) into Eq. (1) and separating the terms at times t and $t-\Delta t$ yields the equation for V at time t:

$$\frac{\partial^2 V}{\partial r^2} + \frac{1}{r}\frac{\partial V}{\partial r} + \frac{1}{r^2}\frac{\partial^2 V}{\partial \phi^2} - AV = g, \tag{A2}$$

with

$$A = \frac{\rho S C_M}{\Delta t},$$

$$g = -\rho S\left(\frac{C_M}{\Delta t}V^{(t-\Delta t)} + I_{ion}^{t-\Delta t/2}\right).$$

The method to calculate $I_{ion}^{t-\Delta t/2} = [I_{ion}(V^{t-\Delta t},(y)^{t-\Delta t}) + I_{ion}(V^{t-\Delta t},(y)^t)]/2$ is described in Ref. [18].

The system is then discretized with respect to the ϕ coordinate with a uniform mesh of N points separated by $\Delta\phi = 2\pi/N$. The partial derivative with respect to ϕ is expressed by a centered finite difference:

$$\frac{\partial^2 V_j(r)}{\partial \phi^2} = \frac{V_{j-1}(r) - 2V_j(r) + V_{j+1}(r)}{\Delta \phi^2},$$

in which j is the index of the node. Since $V(0) = V(2\pi)$, V_j can be expressed as the inverse Fourier transform,

$$V_j(r) = \frac{1}{N}\sum_{m=0}^{N-1} V_m(r) e^{-i(2\pi m/N)j},$$

in which the $V_m(r)$ are the basis functions associated with each spatial frequency. The second derivative $\partial^2 V/\partial\phi^2$ is finally approximated as

$$\frac{\partial^2 V(r, j\Delta\phi)}{\partial \phi^2} = \frac{2}{N\Delta\phi^2}\sum_{m=0}^{N-1} V_m(r) e^{-i(2\pi m/N)j}\left[\cos\left(\frac{2\pi m}{N}\right) - 1\right].$$

The two remaining partial derivatives of Eq. (A2) are

$$\frac{\partial V(r, j\Delta\phi)}{\partial r} = \frac{1}{N}\sum_{m=0}^{N-1} \frac{\partial V_m(r)}{\partial r} e^{-i(2\pi m/N)j},$$

$$\frac{\partial^2 V(r, j\Delta\phi)}{\partial r^2} = \frac{1}{N}\sum_{m=0}^{N-1} \frac{\partial^2 V_m(r)}{\partial r^2} e^{-i(2\pi m/N)j}.$$

Putting these together, all these expressions in Eq. (A2) end up in a set of N second-order ordinary differential equations for the basis function (V_m, $m \in [0, N-1]$) in the Fourier space

$$\frac{d^2V_m}{dr^2}+\frac{1}{r}\frac{dV_m}{dr}+\left\{\frac{2}{r^2\Delta\phi^2}\left[\cos\left(\frac{2\pi m}{N}\right)-1\right]-A\right\}V_m=g_m, \tag{A3}$$

where g_m is the projection of g in the discrete Fourier space. Since V is real, the projection on the Fourier basis is symmetric, which means that there are N equations to solve, corresponding to $N/2$ real parts and $(N/2)-1$ imaginary parts.

Equation (A3) is solved using a finite-element method with a linear basis functions (hat functions) [47]. It yields a system of linear equations of the form $AV=g$, where A is a tridiagonal matrix. The system of equation is solved with a LU decomposition algorithm optimized for tridiagonal matrices [48]. In summary, the method consists in applying, for each time step Δt, the following steps:

(i) Calculate g at each node.
(ii) $g_m(r)=\mathrm{FET}(g(r))$ for each layer r.
(iii) For each $m\in\{0,1,\ldots,N-1\}$, solve $V_m(r)$.
(iv) $V=\mathrm{FFT}^{-1}(V_m)$.

Figure 9 shows the error in the set $\{D,A,T\}$ for a periodic reentry as a function of $\Delta x=2\pi R_{in}/(N-1)$ while changing N. For each value of N, we have also found that a twofold increase of N_r was producing a negligible decrease of ε (less than 0.01%, not shown). In this paper, we use $\Delta t=5$ μs, a radial distance of 80 μm between the layers, and a number of modes in the Fourier basis (N) such that the internode distance of the grid at R_{in} is equal to ~ 67 μm. These values assure a maximum error of less than 2%. The fast Fourier transform (FFT) algorithm used in this paper is the fftw v2.0 (http://www.fftw.org/) included in a C program running on 8 RISC 12000 processors using the OpenMP library.

[1] G. R. Mines, Trans. R. Soc. Can. **4**, 43 (1914).
[2] L. H. Frame, R. L. Page, P. A. Boyden, J. J. Fenoglio, Jr., and B. F. Hoffman, Circulation **76**, 1155 (1987).
[3] L. H. Frame and M. B. Simson, Circulation **78**, 1277 (1988).
[4] J. Brugada, L. Boersma, C. J. Kirchhof, V. V. Heynen, and M. A. Allessie, Circulation **84**, 1296 (1991).
[5] T. Ikeda, M. Yashima, T. Uchida, D. Hough, M. C. Fishbein, W. J. Mandel, P. S. Chen, and H. S. Karagueuzian, Circ. Res. **81**, 753 (1997).
[6] J. M. Davidenko, A. V. Pertsov, R. Salomonsz, W. Baxter, and J. Jalife, Nature (London) **355**, 349 (1992).
[7] R. A. Gray, J. Jalife, A. Panfilov, W. T. Baxter, C. Cabo, J. M. Davidenko, and A. M. Pertsov, Circulation **91**, 2454 (1995).
[8] A. M. Pertsov, E. A. Ermakova, and A. V. Panfilov, Physica D **14**, 117 (1984).
[9] A. Karma, Phys. Rev. Lett. **65**, 2824 (1990).
[10] A. T. Winfree, Chaos **1**, 303 (1991).
[11] I. R. Efimov, V. I. Krinsky, and J. Jalife, Chaos, Solitons Fractals **5**, 513 (1995).
[12] A. Panfilov and P. Hogeweg, Phys. Lett. A **176**, 295 (1993).
[13] M. Courtemanche, Chaos **6**, 579 (1996).
[14] F. H. Samie, O. Berenfeld, J. Anumonwo, S. F. Mironov, S. Udassi, J. Beaumont, S. Taffet, A. M. Pertsov, and J. Jalife, Circ. Res. **89**, 1216 (2001).
[15] F. H. Fenton, E. M. Cherry, H. M. Hastings, and S. J. Evans, Chaos **12**, 852 (2002).
[16] H. Ito and L. Glass, Physica D **56**, 84 (1992).
[17] M. Courtemanche, L. Glass, and J. P. Keener, Phys. Rev. Lett. **70**, 2182 (1993).
[18] A. Vinet and F. A. Roberge, Ann. Biomed. Eng. **22**, 568 (1994).
[19] M. Courtemanche, J. P. Keener, and L. Glass, SIAM J. Appl. Math. **56**, 119 (1996).
[20] P. Comtois and A. Vinet, Phys. Rev. E **68**, 051903 (2003).
[21] E. Cytrynbaum and J. P. Keener, Chaos **12**, 788 (2002).
[22] E. G. Tolkacheva, D. G. Schaeffer, D. J. Gauthier, and W. Krassowska, Phys. Rev. E **67**, 031904 (2003).
[23] E. M. Cherry and F. H. Fenton, Am. J. Physiol. **286**, 2332 (2004).
[24] C. H. Luo and Y. Rudy, Circ. Res. **68**, 1501 (1991).
[25] F. Xie, Z. L. Qu, and A. Garfinkel, Phys. Rev. E **58**, 6355 (1998).
[26] J. P. Keener, SIAM J. Appl. Math. **46**, 1039 (1986).
[27] V. S. Zykov, *Simulation of Wave Processes in Excitable Media* (Manchester University Press, Manchester, 1987).
[28] E. Meron, Phys. Rep. **218**, 1 (1992).
[29] P. Comtois and A. Vinet, Phys. Rev. E **60**, 4619 (1999).
[30] G. W. Beeler and H. Reuter, J. Physiol. (London) **268**, 177 (1977).
[31] A. Vinet, Ann. Biomed. Eng. **28**, 704 (2000).
[32] P. Comtois and A. Vinet, Chaos **12**, 903 (2002).
[33] A. Vinet and F. A. Roberge, J. Theor. Biol. **147**, 377 (1990).
[34] A. Vinet and F. A. Roberge, J. Theor. Biol. **170**, 201 (1994).
[35] A. Vinet and F. A. Roberge, J. Theor. Biol. **170**, 183 (1994).
[36] M. Courtemanche and A. T. Winfree, Int. J. Bifurcation Chaos Appl. Sci. Eng. **1**, 431 (1991).
[37] L. J. Leon, F. A. Roberge, and A. Vinet, Ann. Biomed. Eng. **22**, 592 (1994).
[38] A. Vinet, J. Biol. Syst. **7**, 451 (1999).
[39] N. F. Britton, *Reaction-Diffusion Equations and Their Applications to Biology* (Academic Press, London, 1986).
[40] E. Meron, Physica D **49**, 98 (1991).
[41] Z. Qu, F. Xie, and A. Garfinkel, Ann. Biomed. Eng. **28**, 755 (2000).
[42] M. A. Watanabe, F. H. Fenton, S. J. Evans, H. M. Hastings, and A. Karma, J. Cardiovasc. Electrophysiol. **12**, 196 (2001).
[43] B. Echebarria and A. Karma, Phys. Rev. Lett. **88**, 208101 (2002).
[44] N. Otani, Chaos **12**, 829 (2002).
[45] I. V. Biktasheva and V. N. Biktashev, Phys. Rev. E **67**, 026221 (2003).
[46] T. J. Wu, S. F. Lin, J. N. Weiss, C. T. Ting, and P. S. Chen, Circulation **106**, 1859 (2002).
[47] D. H. Norrie and G. De Vries, *An Introduction to Finite Element Analysis* (Academic Press, New York, 1978).
[48] W. H. Press, *Numerical Recipes in C the Art of Scientific Computing* (Cambridge University Press, Cambridge, England, 2000).